Arab J Sci Eng (2016) 41:5215–5231
DOI 10.1007/s13369-016-2242-z

RESEARCH ARTICLE - MECHANICAL ENGINEERING

Multi-objective Optimal Design of a 2-DOF Flexure-Based Mechanism Using Hybrid Approach of Grey-Taguchi Coupled Response Surface Methodology and Entropy Measurement

Shyh-Chour Huang[1] · **Thanh-Phong Dao**[2,3]

Received: 4 January 2016 / Accepted: 8 June 2016 / Published online: 28 June 2016

Abstract A large displacement and a high first natural frequency are two main concerns for any flexure-based positioning system. A two-degree-of-freedom (DOF) flexure-based mechanism (FBM) with a modified double-lever amplification mechanism is first designed. This study then proposes a multi-objective optimal design of the 2-DOF FBM using the hybrid approach of grey-Taguchi coupled response surface methodology and entropy measurement. The design variables of the 2-DOF FBM include the thickness of the flexure hinges and the length of lever amplification, both of which play vital roles in determining quality responses. The quality responses of the 2-DOF FBM are assessed by measuring the displacement and first natural frequency. The experimental plan is carried out using the Taguchi L_{25} orthogonal array. An integrated approach of grey-Taguchi- based response surface methodology and entropy measurement is then applied for the multi-objective optimization of the 2-DOF FBM. To illustrate the relation between the design variables and the output responses, mathematical regression models are developed. The entropy measurement technique is applied to calculate the weight factor corresponding to each response. Then, an analysis of variance (ANOVA) is conducted to determine the significant parameters affecting the responses. In addition, the ANOVA and experimental validations are conducted to validate the statistical adequacy and the prediction accuracy of the developed mathematical models, respectively. The results reveal that the regression models have good statistical adequacy and excellent prediction accuracy. The confirmation results of the grey relational grade fall within 95 % of the confidence interval. It is strongly believed that the proposed approach has great potential for the optimal design of related flexure-based mechanisms.

Keywords 2-DOF flexure-based mechanism · Flexure hinge · Multi-objective optimization · Taguchi method · Response surface methodology · Grey relational analysis · Entropy measurement

1 Introduction

Two-degree-of-freedom (DOF) flexure-based mechanisms (FBMs) can be found in a variety of applications, e.g. biomechanics, ultrahigh- speed machining, micro-electromechanical systems, atomic force microscopes and optical fibre alignment [1–3]. A 2-DOF FBM transfers motions based on the elastic deformations of flexure hinges instead of the traditional mechanical joints. Hence, the 2-DOF FBM offers several extra advantages, such as smooth displacement, no backlash, zero friction, no noise, simplified manufacturing processes, increased precision, increased reliability and monolithic structure.

In recent years, several studies have constructed 2-DOF flexure-based stages. For example, research has been conducted on the kinematics, statics, stiffness, load capacity and dynamics for a 2-DOF compliant mechanism using a pseudo-rigid-body model [4]. The dynamics model of a 2-DOF compliant stage using the Lagrange equation has been analysed [5]. Also, the linear force–deflection relationship

✉ Thanh-Phong Dao
daothanhphong@tdt.edu.vn

[1] Department of Mechanical Engineering, National Kaohsiung University of Applied Sciences, 415 Chien-Kung Road, Kaohsiung 80778, Taiwan, R.O.C

[2] Division of Computational Mechatronics, Institute for Computational Science, Ton Duc Thang University, Ho Chi Minh City, Vietnam

[3] Faculty of Electrical and Electronics Engineering, Ton Duc Thang University, Ho Chi Minh City, Vietnam

and experimentations for the 2-DOF compliant mechanism using the matrix method have been demonstrated [6]. Finite-element analysis (FEA) results indicated the mechanism as having an almost linear force–deflection relationship. An investigation of the displacement and natural frequency of the 2-DOF compliant mechanism using FEA has also been conducted [7]. The displacement, actuation stiffness and output compliance for a 2-DOF compliant micro-gripper using the pseudo-rigid-body model were analysed [8]. The simulation results showed the gripper as having a decoupled translational motion in two axes and a high resonant frequency. The statics, dynamics and workspace for the 2-DOF compliant stage using the matrix method were also studied [9], and a robust motion tracking control of the 2-DOF flexure-based mechanism investigated [10].

In general, the displacement and first natural frequency are the most important quality characteristics for an efficient 2-DOF FBM. Because if the 2-DOF FBM has a large displacement, the workspace is then enlarged; moreover, if the 2-DOF has a high first natural frequency, the responding speed is faster.

In the past, some researchers only focused on the displacement [7,11–13], while others concentrated on the first natural frequency [6,9,14,15]. Unlike previous studies, this study proposes a new 2-DOF FBM that possesses a large displacement and a high first natural frequency, simultaneously. The large displacement can be achieved by using a modified double-lever amplification mechanism. This double-lever amplification mechanism, initially designed for the 2-DOF FBM, has not yet been reported in previous studies. The high frequency can be obtained via adjusting the geometrical dimensions of flexure hinges. To achieve a large displacement and a high first natural frequency for the 2-DOF FBM, a multi-objective strategy is needed in this study.

Before performing the multi-objective optimization problem, a set of experiments are carried out to collect the displacement and first natural frequency data. The experimental plan is constructed by using the orthogonal arrays of Taguchi method [16] because the number of experiments can be minimized instead of a full factorial experiment. The Taguchi method can optimize a single objective but it fails to multi-objective optimization problem. Hence, some researchers have developed many hybrid optimization methodologies to solve the multi-objective optimization problem. For instance, the Taguchi method was integrated with an artificial neural network (ANN), but this method requires voluminous data and tedious training characterized by an uncertainty in finite convergence [17,18]. Besides, the Taguchi method was combined with fuzzy logic analysis; however, fuzzy logic rules do not readily lend themselves to dynamic changes in a process [19,20]. In addition, the Taguchi method was coupled with grey relational analysis (GRA) as a generally the preferred combination, because the grey relational grade is used as the performance measure in GRA and the grade values are maximized irrespective of the nature of the quality characteristics [21,22]. In summary, the Taguchi method and grey relational analysis are chosen for the multi-objective optimization of the 2-DOF FBM in this study. However, in this hybrid approach, the weight factor for each quality characteristic should be determined. The reason is because when the weight factor of each response changes, the setting of the optimal parameters also changes. Hence, the weight factor of each response must be determined accurately. The weight factor can be calculated by the entropy measurement technique [23,24].

In the optimal process, the relationship between the design variables and quality characteristics should be correctly formulated to predict some discrete values. To efficiently demonstrate this relationship, response surface methodology (RSM), a statistical regression technique [25], is used in this study. In the past, the Taguchi method was integrated with RSM for the optimization of the laser beam thin steel sheet cutting process [26,27]. However, the statistical adequacy of predictive models must be tested by means of an analysis of variance (ANOVA) along with the validation experiments and statistical criteria [28]. Moreover, the prediction accuracy of RSM models must also be checked by experimental validation.

The GRA-Taguchi method, RSM and entropy measurement are now used in various areas of multi-response optimization involving coating, plasma, drilling and CNC [29–34]. However, how to best integrate these methods and create a hybrid approach with which complicated problems can be solved remains a challenge. To the best of our knowledge, a hybrid approach incorporating grey-Taguchi-based response surface methodology and the entropy measurement technique for the multi-objective optimal design process of flexure-based mechanisms has yet to be developed.

The aim of this study was to develop the proposed multi-objective optimal design of a new 2-DOF flexure-based mechanism through a hybrid approach combining the grey-Taguchi-based response surface methodology and entropy measurement. The proposed 2-DOF flexure-based mechanism was developed via using the double-lever amplification mechanism. The quality responses of the proposed 2-DOF FBM were assessed by measuring the displacement and the first natural frequency. The experimental plan was designed using the Taguchi L_{25} orthogonal array. A hybrid approach of grey-Taguchi based response surface methodology and entropy measurement was used to optimize both responses simultaneously. Prior to optimization, RSM was applied for modelling the relationship between the design parameters' responses and the grey relational grade. The entropy measurement technique was adopted for calculating the weight factor corresponding to each response. An ANOVA was then conducted to determine the significant parameters affecting

the responses. In addition, an ANOVA and confirmation tests were performed to validate the prediction accuracy and the statistical adequacy of the developed mathematical models. Finally, experimental validations were performed to verify the optimal results.

2 Proposed Design and Optimal Problem Statement

2.1 Structural Design with Modified Double Amplification Levers

The new 2-DOF flexure-based mechanism (2-DOF FBM) with modified amplification levers proposed in this paper, as shown in Fig. 1, comprises the main components as follows: (1) screw holes where the proposed mechanism is fixed by screws; (2) the modified lever amplification mechanism, consisting of two similar levers arranged in a symmetric frame and through a middle point N or M, is called a double-lever amplification mechanism; (3) a pivot flexure hinge connecting the levers with the screw hole is considered to be a rotary joint; (4) a mobile platform based on the flexure hinges to move in the x- and y-directions; and (5) a leaf flexure hinge that connects the levers with the mobile platform. The pivot flexure hinge and the leaf flexure hinge were created with a rectangular cross section to allow for a large displacement.

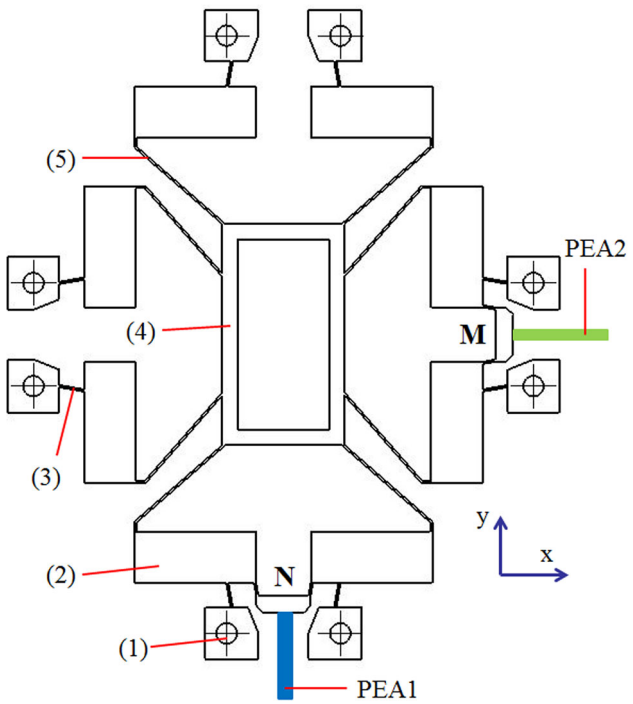

Fig. 1 Proposed design of new 2-DOF FBM

In this study, the piezoelectric actuator (PEA) was adopted as an effective actuator to drive the 2-DOF FBM because of its advantages, such as high resolution, high stiffness and fast frequency. As depicted in Fig. 1, PEA1 (blue colour) acts as a load to a rigid link at middle point N, while PEA2 (green colour) acts as a load to a rigid link at middle point M.

The 2-DOF FBM possesses two working modes that fulfil different requirements. If a positioning is needed along the y-direction, a voltage signal is supplied for PEA1, and then PEA1 exerts the force at point N. Subsequently, through the pivot flexure hinge (3), the levers (2) and the leaf flexure hinge (5), the amplified motion is transferred to the mobile platform (4). If a positioning is needed along the x-direction, a voltage signal is supplied for PEA2, and then, PEA2 applies the force at point M. Through the pivot flexure hinge (3), the levers (2) and the leaf flexure hinge (5), the amplified motion is transferred to the mobile platform (4).

The 2-DOF FBM has a compact size of about 126 by 107 mm and allows planar motion along the x- and y-directions. With the symmetric structure, the 2-DOF FBM creates similar motions in the x-axis and the y-axis. An 8-mm thick Al 7075-T73 was chosen for the proposed mechanism because of its high yield strength to Young's modulus ratio and light relative density. The Young's modulus (E) is 72 GPa, the yield strength (σ_y) is 435 MPa, the Poisson rate (υ) is 0.33 and the density is 2810 kg/m^3.

The most important part of the 2-DOF FBM is the main frame consisting of the double-lever amplification mechanism (2), the pivot flexure hinge (3) and the leaf flexure hinge (5). This is because the main frame is capable of creating a large amplified displacement. A magnified view of the main frame is given in Fig. 2. The geometric design parameters of the main frame affecting the performance characteristics of the proposed mechanism are as follows: (i) thickness of pivot flexure hinge t_1; (ii) thickness of leaf flexure hinge t_2;

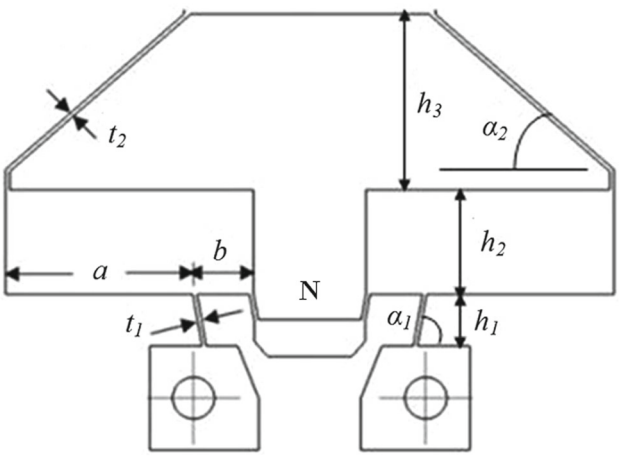

Fig. 2 Magnified view of a mainframe based on double-lever mechanism

and (iii) length of lever amplification mechanism b. The other parameters that are constant because they have little effect on the performance characteristics of the proposed mechanism are as follows: (iv) distances h_1 of 4.92 mm, h_2 of 10 mm and h_3 of 16.82 mm; (v) distance a of 17.8 mm; and (vi) angles α_1 of 80° and α_2 of 41.14°.

In the current work, the 2-DOF FBM design was based on the principle of the double-lever amplification mechanism which would likely amplify the displacement and have the desired high frequency for a fast response. In order to fulfil these requirements, the geometric design parameters of the main frame were optimized by a suitable optimization methodology. Because the 2-DOF FBM has a symmetric structure, the performance characteristics along the x-direction are similar to those along with the y-direction; thus, PEA1 only was used to drive the mobile platform moving along the y-axis to investigate the performance characteristics. When the mobile platform moves, the displacement and the frequency are measured.

2.2 Optimal Problem Statement

The displacement and the first natural frequency are the two most important responses of the proposed 2-DOF FBM. If a mobile platform has a large displacement, then it will have a broad positioning capacity; while if a mobile platform has a high first natural frequency, then it will be capable of rapid response. The displacement and the first natural frequency are considered as two objective functions. This study aimed to find an optimal set of the design variables, such that the FBM has the largest displacement along the y-axis over 0.2 mm and the highest first natural frequency over 1200 Hz. To achieve a large displacement and a high first natural frequency for the proposed 2-DOF FBM, the displacement and the first natural frequency must be optimized simultaneously via a suitable optimization approach. The multi-objective optimization problem for the proposed 2-DOF FBM can be briefly described in the standard form as follows:

Design variables: t_1, t_2, b

Cost functions:

$$\text{Maximize} \quad f_1(t_1, t_2, b) \tag{1}$$

$$\text{Maximize} \quad f_2(t_1, t_2, b) \tag{2}$$

Subject to constraints:

$$\sigma_{\max} \leq \frac{\sigma_y}{SF} \tag{3}$$

$$\begin{cases} 0.4\,\text{mm} \leq t_1 \leq 1.2\,\text{mm} \\ 0.4\,\text{mm} \leq t_2 \leq 1.2\,\text{mm} \\ 4\,\text{mm} \leq b \leq 12\,\text{mm} \end{cases} \tag{4}$$

where f_1 identifies the displacement that is a cost function of design variables (t_1, t_2, b) and f_2 represents the first natural frequency that is a cost function of design variables (t_1, t_2, b); t_1, t_2, b are the geometric design variables of the flexure hinges; $\sigma_{\max}$ denotes the maximum stress of the flexure hinges; SF is the safety factor; and σ_y denotes the yield strength of the proposed material Al 7075-T73.

In general, most flexure-based stages only operate in the elastic area of a specific material [1–15]. To minimize plastic failures, a safety factor as large as possible should be selected. In this study, a safety factor of 2.5 was chosen for the FBM. The design variables were assigned in the range of Eq. (4), because if thicknesses t_1 and t_2 are much lower than 0.4 mm, the displacement will be increased but the frequency decreased. Also, if the thickness is much larger than 1.2 mm, the mass of the stage can increase and the proposed mechanism becomes stiffer; as a result, the travel range will decrease. The lower bounds for the parameters were selected to guarantee compliance, and the upper bounds of the geometric dimensions were set to achieve a compact structure. If the length b is more than 12 mm, the travel amplification ratio will be reduced; if b is ≤4 mm, the mechanism will not be safe at the hinges.

The thickness and width of the flexure hinges are directly related to the optimization problem for the following reasons. In order to create greater motion, the resistance of the flexure hinges must be reduced, which means the thickness of the flexure hinges should be decreased regardless of whether they have circular or rectangular geometries. However, a decrease in the thickness will increase the stress of the flexure hinge [35]. The flexure hinges in this study were subjected to a bending load from PEA1 that created an axis bending moment. For a bending load, according to elastic theory [36], the maximum stress of the flexure hinge is not only related to the axis bending moment but also to the stress concentration. In summary, the maximum stress is related to the axis bending moment, the stress concentration and the geometric parameters of the flexure hinges by the following equation [35,36]:

$$\sigma_{\max} = \frac{6 M_z K_t}{t^2 w} \tag{5}$$

where $\sigma_{\max}$ is the maximum equivalent stress; M_z is the axis bending moment; K_t is the stress concentration factor; t is the thickness variable of the flexure hinges; and w is the thickness of the flexure hinges.

Equation (5) shows that the thickness t has a critical effect on the maximum stress. Reference [35] proved that the width of the flexure hinges has a very small effect on the maximum stress, while the length of the flexure hinges has a relatively large effect on the maximum stress. Hence, in this study, the

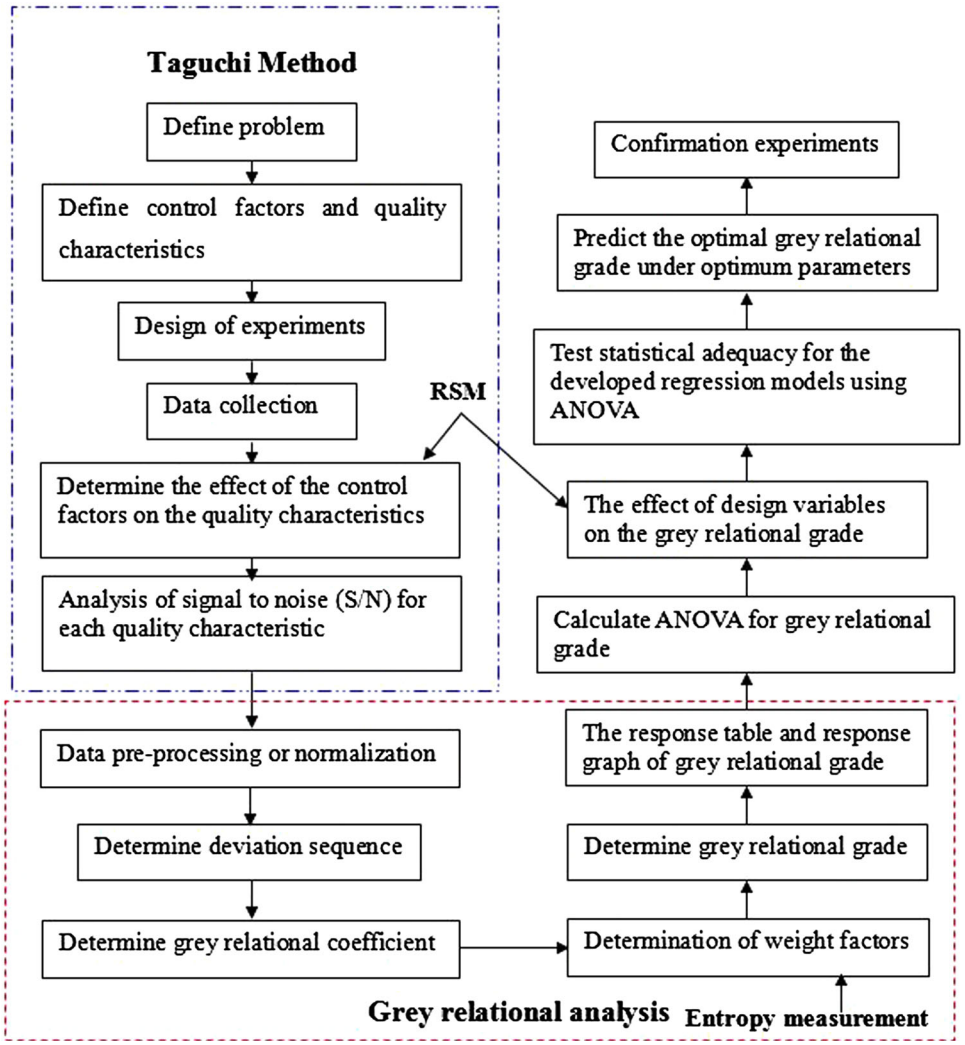

Fig. 3 Flowchart of multi-objective optimal hybrid approach

width of flexure hinges was designed as the constant of w = 8 mm. The optimization problem is carried out to find the optimal parameters of the thickness and length of the flexure hinges so as to achieve the best values of displacement and frequency.

3 Methodology for Optimization

A hybrid integration of the grey-Taguchi-based response surface methodology and entropy measurement technique was adopted as an effective multi-objective optimization tool for the proposed 2-DOF FBM.

Figure 3 shows a stepwise flowchart for the multi-objective optimization methodology using a hybrid approach of grey-Taguchi- based response surface methodology and the entropy measurement technique. The optimization process is divided into key steps as follows:

Step 1 Define problem

The purpose of this study is the optimal design for a new 2-DOF flexure-based mechanism based on the double-lever amplification mechanism. The goal is to develop the mechanism with the best quality objectives. The first quality objective is to maximize the displacement; the second objective is to maximize the first natural frequency.

Step 2 Define control factors and quality characteristics

As mentioned, the thickness of pivot flexure hinge t_1, the thickness of leaf flexure hinge t_2 and the length of lever amplification mechanism b are the control factors for achieving the best quality objectives. The displacement and the first natural frequency of the 2-DOF FBM are two quality characteristics, which will be optimized simultaneously.

Step 3 Design of experiments using the orthogonal array of the Taguchi method

To investigate the entire design parameters with a small number of experiments, the Taguchi method employs a spe-

cial design of the orthogonal array instead of a full factorial approach [16]. Hence, the experimental plan is based on the Taguchi method.

Step 4 Experimental data collection

After experimenting, the displacement and first natural frequency are collected for the next step.

Step 5 Determine the effect of the control factors on the quality characteristics

Response surface methodology (RSM) is adopted to describe the relationship between the design variables and the two quality characteristics. These relationships are investigated by a quadratic polynomial regression model because of its flexibility to an approximate nonlinear response, as compared to first-order models which often result in lack-of-fit; the mathematical model of the quadratic regression model is described below [29]:

$$f = \beta_0 + \sum_{u=1}^{N} \beta_u x_u + \sum_{u=1}^{N} \beta_{uu} x_u^2 + \sum_{u} \sum_{v} \beta_{uv} x_u x_v + \varepsilon \quad (6)$$

where f is the estimated response of the 2-DOF FBM; x_u and x_v represent the design variables of the 2-DOF FBM; β_0 is a constant; β_u ($u = 0, 1, 2, \ldots, N$) is a linear regression coefficient; N is the number of design variables; β_{uu} and β_{uv} are quadratic regression coefficients that can be determined by the least-squares method [30]; and ε denotes the noise or error which is neglected in this study as the experiments are carried out under stable conditions.

Step 6 Analysis of signal to noise (*S/N*) for each quality characteristic

The Taguchi method recommends the loss function. The loss function is then transferred into the signal-to-noise ratio (S/N). The S/N is utilized to determine the deviation between the experimental value of the quality characteristic and the desired value. The quality characteristics of the desired values can be categorized into three types as follows [29–34]: the lower-the-better, the higher-the-better and the nominal-the-better. In this study, a large displacement and a high first natural frequency are the desired quality characteristics for the 2-DOF FBM; hence, the higher-the-better type is adopted for both the displacement and the first natural frequency, calculated as follows:

$$\eta = -10 \log \left(\frac{1}{n} \sum_{i=1}^{n} \frac{1}{f_i^2} \right) \quad (7)$$

where η is the signal to noise in decibels; f_i is the measured response value of the ith experiment; and n is the number of experiments.

According to the Taguchi method, the optimal set of design parameters corresponds to the highest S/N ratio. This is right for a single optimization problem, but not for the multi-objective optimization problem in the present study. As a result, the grey relational analysis is integrated with the Taguchi method to optimize the multiple quality characteristics of the 2-DOF BM. Based on the grey relational analysis, the S/N ratio of each quality characteristic is first normalized in the range between zero and unity in the next step.

Step 7 Data preprocessing or normalization

To avoid the effect of different units and to reduce the variability, data preprocessing or normalization is a necessary step in the grey relational analysis [29–34]. Data preprocessing is a transferring of the original sequence to a comparable sequence in the range from zero to one, which means that the given data sequence is transferred into a dimensionless data sequence.

In this study, the normalized S/N ratio $z_i(k)$ value for n experiments is calculated to adjust the measured values on different scales to a common scale. The type of the higher-the-better is used for both quality responses; hence, the normalization equation for the S/N ratio for both quality responses is computed as follows:

$$z_i(k) = \frac{\eta_i(k) - \min \eta_i(k)}{\max \eta_i(k) - \min \eta_i(k)} \quad (8)$$

where $z_i(k)$is the normalized S/N value for the kth response ($k = 1, 2, \ldots, m$) in the ith experiment (known as the comparability sequence of S/N data); $\eta_i(k)$ indicates the estimated S/N value (known as the original sequence of S/N ratio data); and max $\eta_i(k)$ and min $\eta_i(k)$ are the largest and smallest values of η_i, respectively.

Step 8 Determine deviation sequence

Before calculating the grey relational coefficient, the absolute deviation sequence $z_o(k)$ of the reference sequence and comparability sequence $z_i(k)$ must be determined. The absolute deviation sequence is calculated by equation:

$$\Delta_{oi}(k) = \| z_o(k) - z_i(k) \| \quad (9)$$

where $\Delta_{oi}(k)$ is the absolute difference sequence between $z_o(k)$ and $z_i(k)$; $z_o(k)$ is the reference sequence that presents the ideal value (optimal value, generally equal to 1 in a normalized sequence) for the kth response; and $z_i(k)$ is the comparability sequence.

Step 9 Determine grey relational coefficient

In the grey relational analysis, the grey relational coefficient is calculated to give the

relationship between the optimal and actual normalized experimental results [29–34]. In this study, the grey relational coefficient expresses the relationship between the best and the actual normalized S/N ratios. The grey relational coefficient can be computed as follows:

$$\gamma_i(k) = \frac{\Delta_{\min} + \delta\Delta_{\max}}{\Delta_{oi}(k) + \delta\Delta_{\max}} \tag{10}$$

where $\Delta_{\min}$ is the smallest value of Δ_{oi}; $\Delta_{\max}$ is the largest value of Δ_{oi}; and δ is the distinguishing coefficient ($0 \leq \delta \leq 1$)for adjusting the interval of $\gamma_i(k)$. In this study, a δ of 0.5 is set for the average distribution due to the moderate distinguishing effects and good stability of outcomes.

Step 10 Determination of weight factors

In general, the average grey relational coefficient is the grey relational grade. However, the importance of each quality characteristic is different; hence, the weight factor for each quality characteristic is determined before calculating the grey relational grade. The weight factor can be computed by the entropy measurement technique [24]. As proposed by Wen et al. [24], the mapping function $f_i : [0, 1] \rightarrow [0, 1]$ utilized in the entropy should satisfy the following conditions:

$$f_i(0) = 0 \tag{11}$$

$$f_i(x) = f_i(1 - x) \tag{12}$$

where $f_i(x)$ is the monotonic increase in the range of $x \in (0, 0.5)$.

Hence, the following function $w_e(x)$ can be employed as the mapping function in the entropy measure, yielded as follows:

$$w_e(x) = x\mathrm{e}^{(1-x)} + (1 - x)\mathrm{e}^x - 1 \tag{13}$$

This function achieves the maximum value when $x = 0.5$; the value yielded is

$$w_e(0.5) = \mathrm{e}^{0.5} - 1 = 0.6487$$

To obtain the mapping result in the range [0, 1], Wen et al. [24] defined a new entropy W as:

$$W \equiv \frac{1}{(\mathrm{e}^{0.5} - 1)} \sum_{i=1}^{n} w_e(x_i) \tag{14}$$

Wen et al. [24] then proposed the following steps to calculate the weight factor of each response. The sum of the grey relational coefficient D_k in all sequences of each quality characteristic is calculated by the following equation:

$$D_k = \sum_{i=1}^{n} \gamma_i(k), \quad k = 1, \ldots, m \tag{15}$$

The entropy of each response e_k is calculated as:

$$e_k = K \sum_{i=1}^{n} w_e\left(\frac{\gamma_i(k)}{D_k}\right) \tag{16}$$

where the normalized coefficient K is determined as $K = \frac{1}{(\mathrm{e}^{0.5}-1)\times n} = \frac{1}{0.6487\times n}$.

The sum of entropy E_S is determined by the following equation:

$$E_S = \sum_{k=1}^{m} e_k \tag{17}$$

The normalized weight of each quality response w_k is calculated as:

$$w_k = \frac{1}{m - E_S} \times \frac{1 - e_k}{\sum_{k=1}^{m} \frac{1}{m-E_S}(1 - e_k)} \tag{18}$$

where $\lambda_k = \frac{1-e_k}{m-E_S}$ is the relative weighting coefficient.

Step 11 Determine the grey relational grade

The grey relational grade (GRG) is computed by finding the mean of the grey relational coefficient values. The grey relational grade values are taken as the single representative for multiple responses. The grey relational grade reflects the degree of influence between the comparability sequence and the reference sequence. If the grey relational grade is equal to unity, it implies the sequences are identical and all have values equal to unity. A high grey relational grade corresponds to a strong relational degree between the original sequence and the reference sequence, and yields the factor combinations closer to the optimal setting. The mathematical grey relational grade is calculated by the following equation [24]:

$$\psi_i = \frac{1}{\mathrm{m}} \sum_{k=1}^{m} \gamma_i(k) \tag{19}$$

However, the relative significance of the responses varies as per requirement. In practice, all responses have unequal weights. Hence, the grey relational grade can be determined by multiplying the grey relational coefficients with the corresponding weight factors of the quality characteristics [24]:

$$\psi_i = \sum_{k=1}^{m} w_k \gamma_i(k) \tag{20}$$

where $\sum_{k=1}^{m} w_k = 1$; and w_k denotes the weight factor for the kth quality characteristic. The total of the weights is equal to zero:

$$\sum_{k=1}^{m} w_k = 1 \tag{21}$$

Step 12 Response table and response graph of grey relational grade

Based on the response table and response graph of the grey relational grade through the Taguchi method, the optimal parameters are determined.

Step 13 Calculate ANOVA for grey relational grade

An analysis of variance (ANOVA) is used to estimate the significance of each factor on the grey relational grade.

Step 14 Effect of design variables on the grey relational grade

In this step, RSM is used to describe the relationship between the design variables and the grey relational grade. From that, the effect of the design variables on the grey relational grade can be determined using Eq. (6).

Step 15 Test statistical adequacy and prediction accuracy for the developed regression models

An analysis of variance (ANOVA) is used to test statistical adequacy for the developed regression models.

In addition, to validate the prediction accuracy of the developed models, the design variables are selected randomly in their ranges to manufacture the prototypes needed to carry out the corresponding experiments.

Step 16 Predict the optimal grey relational grade under the optimum parameters

The optimal grey relational grade is predicted by considering the effect of all parameters or the most significant parameter. The estimated mean of the grey relational grade can be determined as follows:

$$\mu_{\mathrm{G}} = G_{\mathrm{m}} + \sum_{s=1}^{g} (G_{\mathrm{o}} - G_{\mathrm{m}}) \tag{22}$$

where μ_{G} is the optimal GRG value of the predicted mean; G_{m} is the total mean of the grey relational grade; G_{o} is the optimal mean grey relational grade for each level of factor; and q is the number of significant parameters affecting the grey relational grade.

In order to judge the closeness of the observed value with the predicted value, the confidence interval (CI) value of the predicted value for the optimum factor level combination is determined. The 95 % confidence interval (CI) of the confirmation experiments is calculated using the following equation [16]:

$$\mathrm{CI}_{CE} = \pm\sqrt{F_{\alpha}\,(1, f_e)\, V_e \left(\frac{1}{n_{\mathrm{eff}}} + \frac{1}{R_e}\right)} \tag{23}$$

where α = risk = 0.05; $F_{\alpha}\,(1, f_e) = F_{0.05}\,(1, f_e)$ is the F-ratio at a 95 % $(1-\alpha)$ confidence interval against degrees of freedom 1 and degrees of freedom of error f_{e} [16]; V_{e} is the variance of error (get from ANOVA); $n_{\mathrm{eff}} = n/\,(1+d)$ with n is the total experimental number in the orthogonal array and d is the total degrees of freedom of factors associated in estimates of the mean μ_{G}; and R_{e} is the number of repetitions for the confirmation experiments.

Step 17 Confirmation experiments

The confirmation experiments are the final step for evaluating the prediction accuracy of the developed regression models and validating the optimal results.

4 Results and Discussion

4.1 Experimental Measurements

The relationship between three design variables and the two quality characteristics of the 2-DOF FBM was determined in order to obtain the optimal parameters. First, the composition of the various factors and level values were designed based on the Taguchi method, as given in Table 1.

Because the proposed 2-DOF FBM requires a large displacement for a large workspace and a high first natural frequency for a fast response, this study selected the larger-the-better for the two responses according to the Taguchi method. With three process parameters and five levels, the experimental plan was designed using the L_{25} orthogonal array of the Taguchi method, as shown in Table 2. The 25 experimental tests were conducted to collect the data on the displacement and first natural frequency. The experimental equipment was installed on a vibration isolated optical table (Daeil Systems, Model: DVIO-I-1209M-100t, Korea) to avoid any unexpected vibrations. The prototypes were fabricated using wire electrical discharge machining.

The experimental setup of the displacement is shown in Fig. 4. A high-speed bipolar amplifier (Model HAS 4011, NF Corporation) was utilized to drive the PEA1 (Model 150/5/40 VS10, Piezomechanik GmbH). Retro-reflective tape (Ono Sokki Company) was attached at the top of each thin aluminium beam; this aluminium leaf was then fixed to the mobile platform using screws. A preload was applied on PEA1. A laser vibrometer sensor (Model LV-170, Ono Sokki Company) with a high nanoscale resolution was used to measure the displacement. A frequency response analyser (Model FRA 5097, NF Corporation) was used. Frequency

Table 1 Control factors and their levels

Design variable (mm)	Coded	Levels				
		Level 1	Level 2	Level 3	Level 4	Level 5
t_1	A	0.4	0.6	0.8	1.0	1.2
t_2	B	0.4	0.6	0.8	1.0	1.2
b	C	4	6	8	10	12

Table 2 Design of experiments

No. trial	t_1 (mm)	t_2 (mm)	b (mm)
1	0.4	0.4	4.0
2	0.4	0.6	6.0
3	0.4	0.8	8.0
4	0.4	1.0	10.0
5	0.4	1.2	12.0
6	0.6	0.4	6.0
7	0.6	0.6	8.0
8	0.6	0.8	10.0
9	0.6	1.0	12.0
10	0.6	1.2	4.0
11	0.8	0.4	8.0
12	0.8	0.6	10.0
13	0.8	0.8	12.0
14	0.8	1.0	4.0
15	0.8	1.2	6.0
16	1.0	0.4	10.0
17	1.0	0.6	12.0
18	1.0	0.8	4.0
19	1.0	1.0	6.0
20	1.0	1.2	8.0
21	1.2	0.4	12.0
22	1.2	0.6	4.0
23	1.2	0.8	6.0
24	1.2	1.0	8.0
25	1.2	1.2	10.0

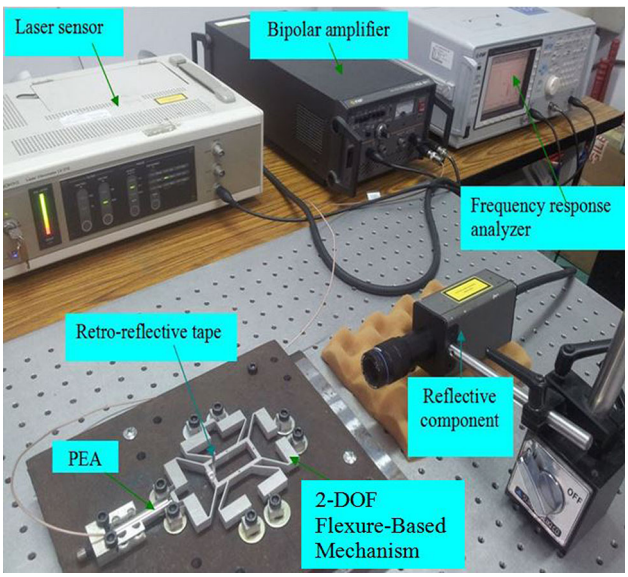

Fig. 4 Experimental measurement of displacement response

response analyser (FRA) display software was installed in the computer. Using the FRA display software, the data were displayed diagrammatically. The experiments were conducted for each of the 25 samples. Each experiment was repeated four times to get the average of the measured values.

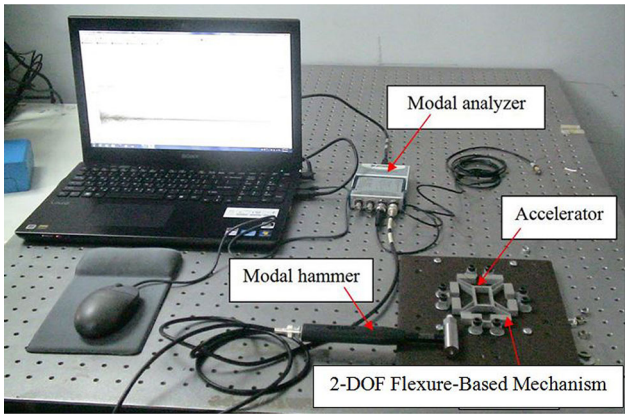

Fig. 5 Experimental measurement of frequency response

The experimental setup of the first natural frequency is shown in Fig. 5. The measurements of the first natural frequency, within the range of 50 Hz–1 kHz, were taken to evaluate the dynamic characteristics of the 2-DOF FBM. A modal hammer (Model 9722A2000-SN 2116555, Kistler) was used to apply the excitation to the mechanism, and the frequency response was measured using an accelerator (Model 4744892, Kistler. The accelerator was attached to be opposite the excitation from the modal hammer. A modal analyser (Model NI USB 9162, National Instruments) was utilized in the data acquisition and analysis. At the end of the hammer, a force sensor was attached to measure the applied force from the hammer. CUTPRO software was installed in a computer to analyse the data. The experiments were conducted for each of the 25 samples. Each experiment was repeated five times. The first natural frequency was measured for the y-axis. The experimental data and signal-to-noise ratios of the two responses are shown in Table 3.

4.2 Effect of Design Variables on Quality Responses

Prior to an optimization problem, the effects of the control parameters on the quality characteristics are critically investigated. A second-order polynomial model was developed to explain the effects of the parameters on the quality characteristics of the 2-DOF FBM. RSM was used to illustrate this relationship. After eliminating the insignificant terms ('Prob > F' larger than 0.05) of the parameters, precise mathematical models for the displacement and frequency were achieved. The mathematical models were developed based on the collected data from the 25 experiments and using Eq. (6).

The mathematical model of the displacement is derived as follows:

Table 3 Experimental average results and *S/N* ratios of two responses

No. trial	f_1 (mm)	*S/N* of f_1	f_2 (Hz)	*S/N* of f_2
1	0.246	−12.1813	567.892	55.0853
2	0.202	−13.8930	793.312	57.9889
3	0.154	−16.2496	1018.732	60.1612
4	0.114	−18.8619	1244.152	61.8975
5	0.065	−23.7417	1469.572	63.3438
6	0.192	−14.3340	613.848	55.7612
7	0.142	−16.9542	839.268	58.4780
8	0.103	−19.7433	1064.688	60.5444
9	0.052	−25.6799	1290.108	62.2125
10	0.280	−11.0568	1348.828	62.5991
11	0.130	−17.7211	659.804	56.3883
12	0.084	−21.5144	885.224	58.9411
13	0.059	−24.5830	1110.644	60.9115
14	0.266	−11.5024	1259.000	62.0005
15	0.220	−13.1515	1357.000	62.6516
16	0.076	−22.3837	705.760	56.9731
17	0.046	−26.7448	931.180	59.3807
18	0.258	−11.7676	989.900	59.9118
19	0.211	−13.5144	1215.320	61.6938
20	0.162	−15.8097	1440.740	63.1717
21	0.073	−22.7335	751.716	57.5211
22	0.240	−12.3958	810.436	58.1744
23	0.194	−14.2440	1035.856	60.3060
24	0.151	−16.4205	1261.276	62.0162
25	0.107	−19.4123	1486.696	63.4444

$$f_1 = 395.14 - 37.33t_1 - 2.68t_2 - 36.13b + 20.5t_1^2 + 21.21t_2^2 + 0.68b^2 \quad (24)$$

The mathematical model of the first natural frequency is derived as follows:

$$f_2 = 93.72 + 122.34t_1 + 1056.21t_2 + 2.85b - 37.04t_1^2 - 59t_2^2 + 0.78b^2 \quad (25)$$

Three-dimensional plots (response surface) illustrating the effects of the design variables on the displacement and first natural frequency were drawn based on the mathematical models.

As shown in Fig. 6a, the displacement lowered rapidly with an increase in thickness t_1. The displacement significantly increased with an increase in thickness t_2 (about 0.75 mm), and then gradually decreased with a further increase in thickness t_2 (up to 1.2 mm). This meant that the displacement varied with a change in thicknesses t_1, t_2.

As seen in Fig. 6b, the displacement sharply decreased with an increase in length b. The displacement varied primarily a nonlinear manner with an increase in thickness t_2. As a result, these parameters could be optimized to maximize the displacement for the 2-DOF FBM.

As depicted in Fig. 6c, the first natural frequency gradually increased with an increase in thickness t_1, and then sharply increased with an increase in thickness t_2. This indicated that the first natural frequency varied with changes in thicknesses t_1 and t_2.

As seen in Fig. 6d, the first natural frequency gradually increased with an increase in length b, but then rapidly increased with an increase in thickness t_2. This indicated that the first natural frequency varied with a change in thickness of t_2 and length b.

From the discussion above, the three design variables all affected the two quality characteristics. However, the maximum value of the displacement conflicted with the maximum value of the first natural frequency corresponding to the design variables. Thus, the aim of this study was to find the optimal combination of processing parameters in order to maximize the displacement and first natural frequency simultaneously.

4.3 Multi-objective Optimization

After conducting the experiments for the displacement and the first natural frequency, the experimental data were transferred into the S/N ratio using Eq. (7); the results are shown in Table 3. The S/N ratio values were normalized using Eq. (8), and the results are given in Table 4.

Next, the deviation sequence was determined using Eq. (9), the grey relational coefficient was calculated using Eq. (10) and the normalized weight factor of each response was computed using Eqs. (11–18). The results are shown in Table 4. By using Eqs. (11–18), the weight factor of the displacement was determined to be 0.5 and that of the first natural frequency to be 0.5. The grey relational grade was then determined using Eqs. (19–20), as shown in Table 4. From Eqs. 9–21, k in brackets (k) represents various responses. The displacement response corresponds to $k = 1$, while the frequency response corresponds to $k = 2$. For example, z_i (1) is the normalized S/N of the displacement and z_i (2) is the normalized S/N of the frequency. $\Delta_{oi}(1)$ and Δ_{oi} (2) are deviation sequences of the displacement and frequency, respectively. γ_i (1) and γ_i (2) are the grey relational coefficients of the deviation sequences of the displacement and frequency, respectively. In Table 4, Δ_{min} is equal to zero (the smallest value of Δ_{oi}) and Δ_{max} is equal to one (the largest value of Δ_{oi}).

As known, the highest grey relational grade in a sequence indicates the closest value to the desired value of the quality response. Therefore, in this study a plot was drawn of the grey relational grade value corresponding to each experiment, as depicted in Fig. 7. As can be clearly observed in Table 4 and

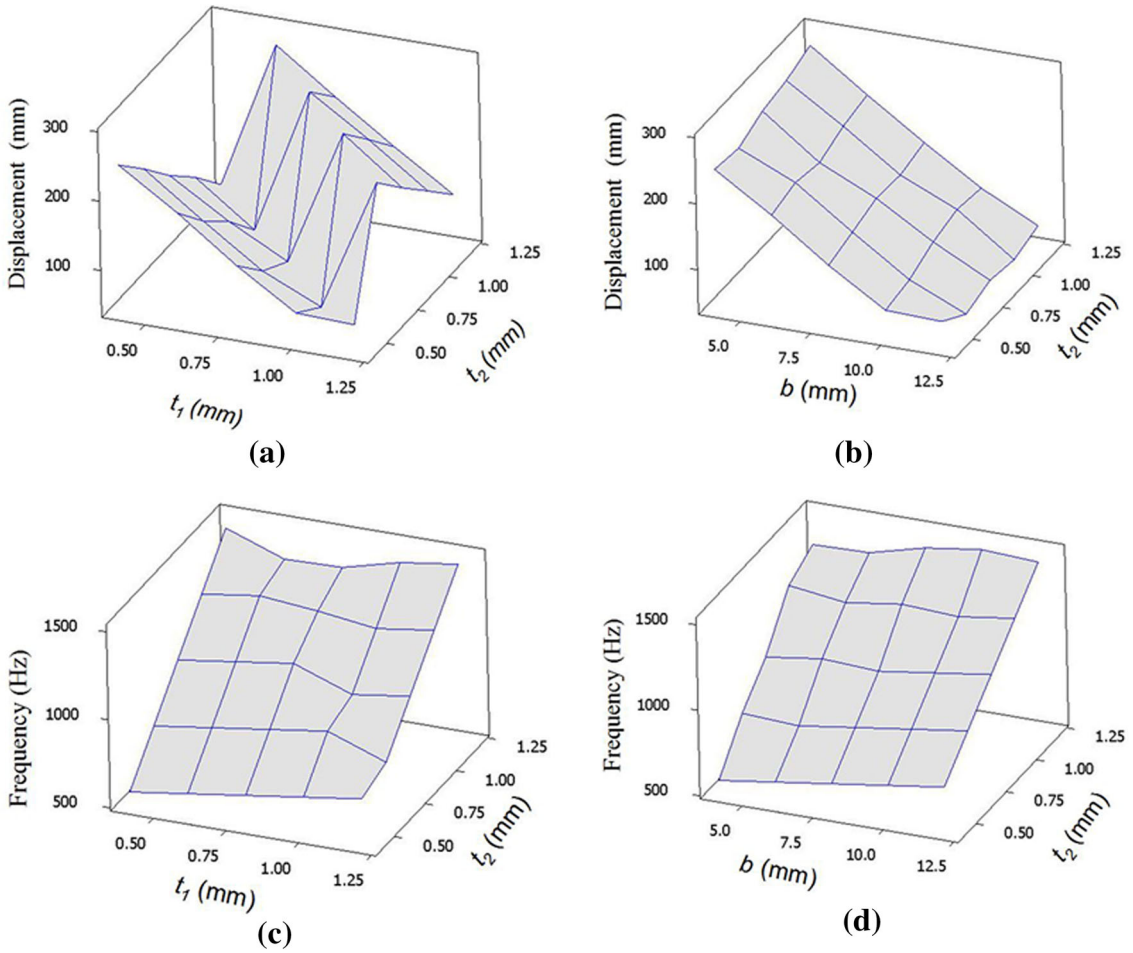

Fig. 6 Surface plots: **a** displacement versus t_1 and t_2; **b** displacement versus t_2 and b; **c** frequency versus t_1 and t_2; **d** frequency versus t_2 and b

Fig. 7, the maximum value of GRG was observed at the 10th experiment, which indicated that the optimal setting of the parameters was close to that used in the 10th experiment.

Using the theory of the Taguchi method, the average grey relational grade for each input parameter level was calculated, as shown in Table 5. The response graph for the average grey relational grade at each parameter level was plotted, as in Fig. 8. The results from Table 5 and Fig. 8 indicated the optimal input parameter level to be A5B5C1 corresponding to thickness t_1 at level 5 (1.2 mm), thickness t_2 at level 5 (1.2 mm) and length b at level 1 (4 mm). The results showed that the maximum displacement was equal to 0.276 mm and the maximum first natural frequency equal to 1261.562 Hz.

4.4 ANOVA for Grey Relational Grade

According to Step 13, an ANOVA was computed to identify the influence of the design parameters on the quality characteristics. As Table 6 shows, factor B (thickness t_2) had the most significant influence on the target characteristics with a percentage contribution of 63.0313 %, followed by factor C (length b) with a percentage contribution of 35.8364 %. Factor A (thickness t_1) had the lowest influence. Therefore, factor A was pooled into the error.

4.5 Effect of Design Variables on Grey Relational Grade

According to Step 14, a polynomial regression equation for the grey relational grade (GRG), constructed using Eq. (6), explained the relationship between the input parameters and the GRG. After eliminating the insignificant terms ('Prob > F' larger than 0.05) of the parameters, the final mathematical model for the GRG was precisely achieved. The mathematical model was developed based on the GRG data from the 25 experiments. The mathematical model of the GRG is developed as follows:

$$\begin{aligned}\mathrm{GRG} = {} & 0.806585 - 0.108418t_1 + 0.105496t_2 - 0.0675306b \\ & + 0.0349643t_1^2 + 0.188976t_2^2 + 0.00192738\mathrm{b}^2 \\ & - 0.0141667t_1t_2 + 0.00925476t_1b \end{aligned} \quad (26)$$

Table 4 Grey generation data of each sequence, difference sequence, grey relational coefficient, grey relational grade and rank of grey relational grade

No.	z_i (1)	z_i (2)	Δ_{oi} (1)	Δ_{oi} (2)	γ_i (1)	γ_i (2)	ψ_i	Rank
1	0.9283	0.0000	0.0717	1.0000	0.8746	0.3333	0.6040	13
2	0.8192	0.3474	0.1808	0.6526	0.7344	0.4338	0.5841	14
3	0.6690	0.6072	0.3310	0.3928	0.6017	0.5601	0.5809	15
4	0.5025	0.8149	0.4975	0.1851	0.5012	0.7299	0.6156	12
5	0.1914	0.9880	0.8086	0.0120	0.3821	0.9765	0.6793	8
6	0.7911	0.0809	0.2089	0.9191	0.7053	0.3523	0.5288	18
7	0.6241	0.4059	0.3759	0.5941	0.5708	0.4570	0.5139	19
8	0.4463	0.6531	0.5537	0.3469	0.4745	0.5904	0.5324	17
9	0.0679	0.8526	0.9321	0.1474	0.3491	0.7724	0.5607	16
10	1.0000	0.8989	0.0000	0.1011	1.0000	0.8318	0.9159	1
11	0.5752	0.1559	0.4248	0.8441	0.5407	0.3720	0.4563	21
12	0.3334	0.4613	0.6666	0.5387	0.4286	0.4814	0.4550	22
13	0.1378	0.6970	0.8622	0.3030	0.3671	0.6227	0.4949	20
14	0.9716	0.8273	0.0284	0.1727	0.9463	0.7432	0.8447	2
15	0.8665	0.9052	0.1335	0.0948	0.7892	0.8406	0.8149	3
16	0.2780	0.2258	0.7220	0.7742	0.4092	0.3924	0.4008	25
17	0.0000	0.5139	1.0000	0.4861	0.3333	0.5070	0.4202	23
18	0.9547	0.5774	0.0453	0.4226	0.9169	0.5419	0.7294	7
19	0.8434	0.7906	0.1566	0.2094	0.7614	0.7048	0.7331	6
20	0.6970	0.9674	0.3030	0.0326	0.6227	0.9387	0.7807	4
21	0.2557	0.2914	0.7443	0.7086	0.4018	0.4137	0.4078	24
22	0.9147	0.3695	0.0853	0.6305	0.8542	0.4423	0.6482	10
23	0.7968	0.6245	0.2032	0.3755	0.7111	0.5711	0.6411	11
24	0.6581	0.8291	0.3419	0.1709	0.5939	0.7453	0.6696	9
25	0.4674	1.0000	0.5326	0.0000	0.4842	1.0000	0.7421	5

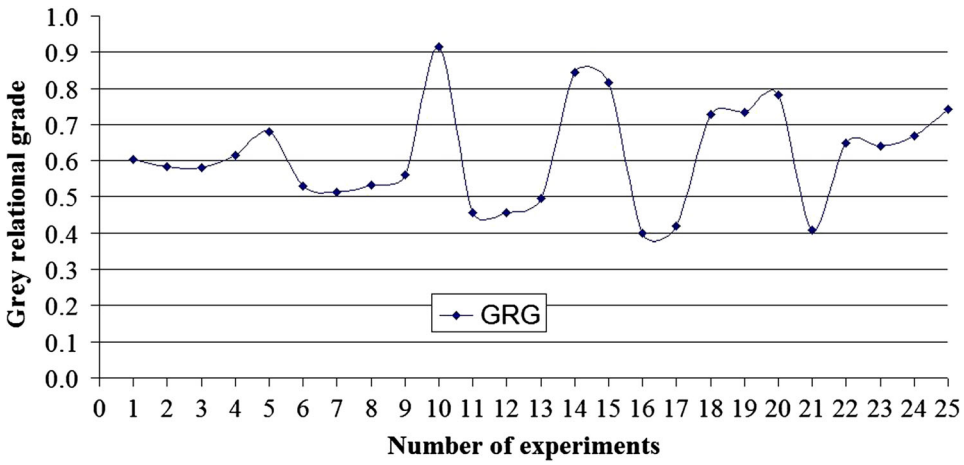

Fig. 7 Plot of GRG values for various experiments

Table 5 Response table for average GRG for each parameter level

Factors	Mean of GRG for each level of each parameter					Max-min	Rank
	Level 1	Level 2	Level 3	Level 4	Level 5		
A	0.613	0.610	0.613	0.613	0.622	−0.0001	2
B	0.480	0.524	0.596	0.685	0.787	−0.1162	3
C	0.748	0.660	0.600	0.549	0.513	0.2359	1

Total mean value of GRG is 0.5185

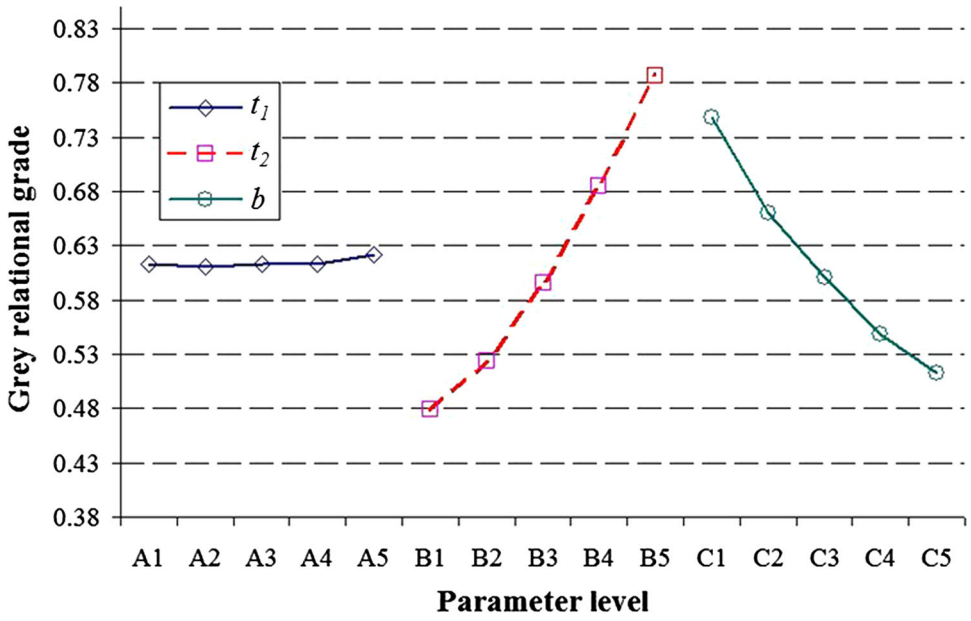

Fig. 8 Response graph of grey relational grade

Table 6 Pooled ANOVA for GRG

Factors	DOF	SS	V	SS'	P (%)
A	4	Pooled			
B	4	0.3063	0.0766	0.3053	63.0313
C	4	0.1745	0.0436	0.1736	35.8364
Pooled error	12	0.0037	0.0002	0.1498	1.1323
Total	24				100

Significant at 95 % confidence level

The two-dimensional contour plots demonstrated the effect of the control factors on the GRG. The grey relational grey could be predicted based on the various colours. As seen in Fig. 9a–c, the GRG was ≤0.4 corresponding to white colour contours. The GRG gradually increased to more than 0.9 corresponding to the most bold green colour areas. The larger the GRG, the better the quality characteristics.

4.6 Statistical Adequacy of Developed Models

According to Step 15, an ANOVA was used to check the statistical adequacy of the developed mathematical models (Eqs. 24–26). The ANOVA was utilized to determine the significance of the coefficients and the fitness of the developed models. Based on the results of the ANOVA, the *F*-value and *p* value were used to test the adequacy of the developed mathematical models, including the displacement, frequency and GRG models. The significance of the model terms is proved when the computed *F*-value is higher than the critical *F*-value tabulated from the standard table at a 95 % confidence level [38] and the 'Prob>F' (*p* value) is less than 0.05. The fitness of the model is tested based on the determination coefficient (*R*-squared value) and *R*-squared (adjusted) [16].

By using the regression method, the insignificant model terms were eliminated. The ANOVA results for the reduced quadratic models, given in Tables 7, 8 and 9, illustrate the significant model terms. These results indicated that the *F*-value of the models proved their significance because the computed *F*-value of each of the model terms was higher than the critical *F*-value tabulated from the standard table at a 95 % confidence level [38]. The results showed the *p* value of the source of the regression models and coefficients to be less than 0.007. The ANOVA results showed the developed models (f_1, f_2, and GRG) to be significant and adequate. The R-squared value for the three models was close to utility, as shown in Tables 7, 8 and 9, representing the excellent fit of the experimental data to the developed mathematical models.

4.7 Prediction Accuracy of Developed Model

According to Step 15, the prediction accuracy of the developed models was confirmed using the experimental investigation. The parameters t_1 of 0.45 mm, t_2 of 0.55 mm and b of 6.5 mm were selected randomly in their ranges (Table 1) to manufacture the four prototypes. These parameter levels were substituted into Eqs. (24–26) to achieve the mean predicted value for each mathematical model. The prototypes were manufactured, and each validation experiment was conducted four times to obtain the mean actual value for each

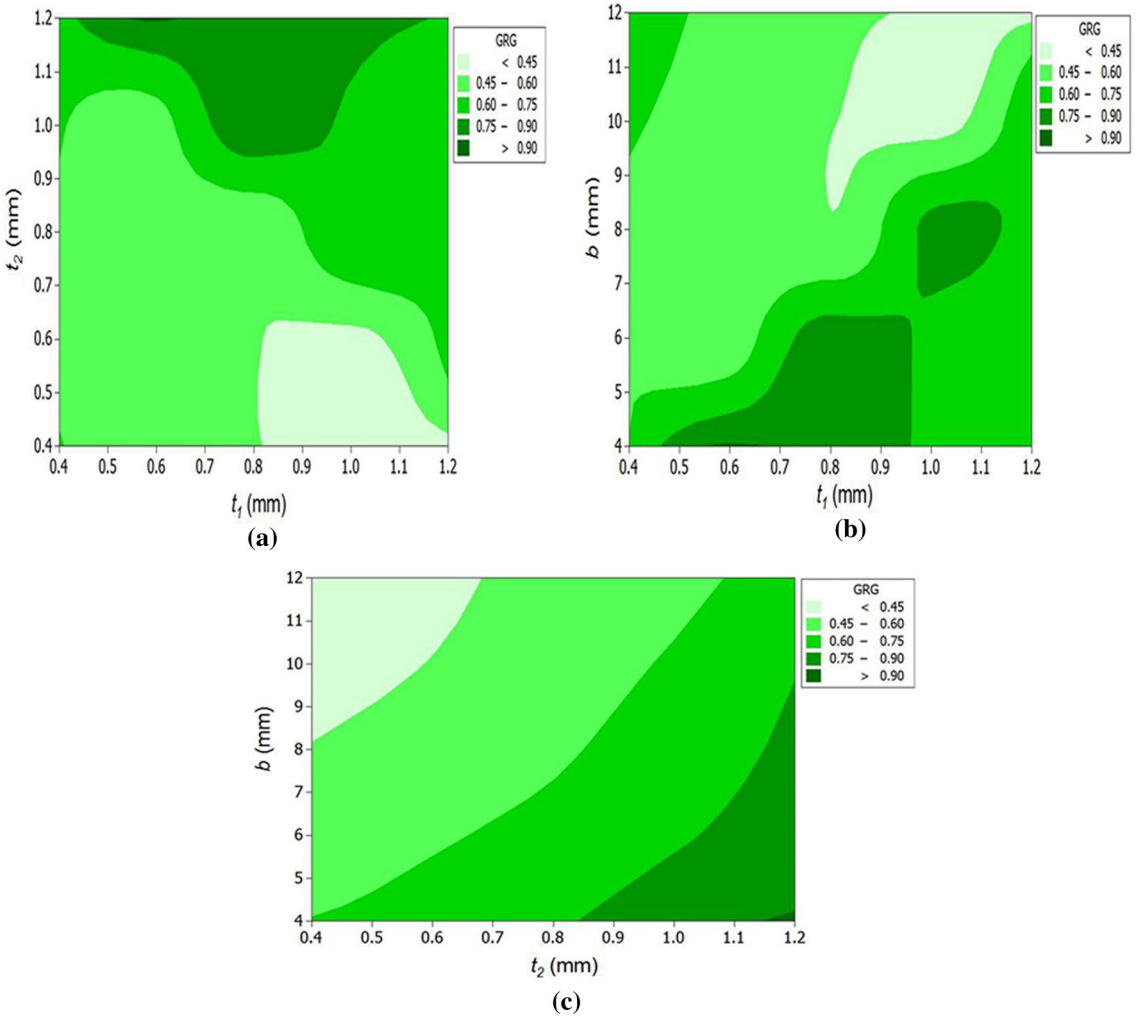

Fig. 9 Contour plots: **a** GRG versus t_1 and t_2; **b** GRG versus t_1 and b; **c** GRG versus t_2 and b

Table 7 ANOVA result for response surface model of displacement

Source	DOF	*F*-value	*p* value	Remark
Regression	6	232.37	0.000	Significant
Linear	3	20.17	0.000	Significant
b	1	59.88	0.000	Significant
$b \times b$	1	5.55	0.030	Significant
Residual error	18			
Total	24			

R-Squared = 98.73 %; *R*-Squared (adjusted) = 98.30 %

Table 8 ANOVA result for response surface model of frequency

Source	DOF	*F*-value	*p* value	Remark
Regression	6	739.30	0.000	Significant
Linear	3	37.58	0.000	Significant
t_2	1	111.16	0.005	Significant
Residual error	18			
Total	24			

R-squared = 99.60 %; *R*-squared (adjusted) = 99.46 %

model. The predicted results were then compared with the actual results to validate the prediction accuracy of the developed models. As shown in Table 10, the results indicated that the deviation errors between the mean predicted results and the mean actual results were less than 7 %, confirming the predictability of the developed mathematical models to be reliably accurate.

4.8 Predict the Optimal Grey Relational Grade Under Optimum Parameters

According to Step 16, the optimal grey relational grade was predicted considering the effect of all control parameters at the optimal level A5B5C1. The estimated mean of the grey relational grade was determined using Eq. 22, and then, the

Table 9 ANOVA result for response surface model of GRG

Source	DOF	*F*-value	*p* value	Remark
Regression	8	356.05	0.000	Significant
Linear	3	709.61	0.000	Significant
t_2	1	1501.87	0.001	Significant
b	1	819.39	0.007	Significant
Square	4	10.99	0.000	Significant
$t_2 \times t_2$	1	17.74	0.001	Significant
b	1	18.45	0.001	Significant
Residual error	12			
Total	24			

R-squared = 99.44 %; *R*-squared (adjusted) = 99.46 %

Table 10 Comparison between predicted and actual responses

Model	Mean predicted value	Mean actual value	Error (%)
f_1	0.182 mm	0.185 mm	2.6 %
f_2	721.037 Hz	737.995	2.3 %
GRG	0.5459	0.5863	6.8 %

95 % confidence interval (CI) of the confirmation experiments was calculated using Eq. 22.

The expected mean value of the four confirmation experiments was obtained as follows: $\mu_G = 0.5185$, $F_{0.05}\,(1, 12) = 4.7472$ (tabulated from standard table in [38]; $V_e = 0.0002$ (get from Table 7); $n_{\text{eff}} = 25/\,(1 + 12) = 1.923$, $Re = 4$; $CI = \pm 0.027$.

$$0.4915 \leq \mu_{\text{confirmation}} \leq 0.5500 \tag{27}$$

4.9 Experimental Validation

According to Step 17, by using the optimal combination A5B5C1, the four experimental validations were performed to validate the optimal results. And then, the finite-element method (FEM) in ANSYS was used to validate the optimal results. Four solid models of the 2-DOF FBM were constructed in Solid works. And then, the automatically method was utilized for meshing the model, and then, each flexure hinge was refined to achieve the analysis accuracy. The 10-node tetrahedral structural solid element of SOLID 92 type was adopted for the meshed model because the SoLID 92 was well suitable for irregular meshes. The Skewness criterion [16] was applied to evaluate the element quality.

As given in Table 11, the GRG value was equal to 0.5185 that was predicted by the proposed hybrid optimization methodology, it was approximately 0.5334 that was determined from the actual experiments, and it was about 0.5467 that was calculated via the FEM in ANSYS. These GRG values fell within 95 % of the CI (see in Eq. 27). In addition, as seen in Table 11, the error between the FEM and the predicted value is less than 6 %. Moreover, the error between the actual and the predicted value is less than 3 %. These errors were came from the manufacturing and assemble errors. In summary, these GRG values fell within 95 % of the *CI* and the errors were relatively low. It could be concluded that the hybrid optimization methodology is an effectively robust technique for multi-objective optimization of the 2-DOF FBM.

Compared with initially desired design (seen in Sect. 2.2), the optimal displacement (0.284 mm) was about 42 % greater than the initial displacement (0.2 mm) and the optimal frequency (1293.812 Hz) was approximately 7.8 % higher than the initial frequency (1200 Hz). It was clearly proved that the quality characteristics of the 2-DOF FBM are efficiently improved by using the hybrid optimization methodology.

5 Conclusions

A 2-DOF flexure-based mechanism with a modified double-lever amplification mechanism was proposed in this study. Then, this study has attempted to conduct a multi-objective optimal design of 2-DOF flexure-based mechanism. The various thicknesses of flexure hinges and the length of lever amplification mechanism were the key design variables. The displacement and first natural frequency were the two responses of the 2-DOF flexure-based mechanism.

An integrated approach of grey-Taguchi-based response surface methodology and entropy measurement was adopted for multi-response optimization to overcome the disadvantages of the Taguchi method in the multiple quality optimization. Response surface methodology was used for

Table 11 Predicted and validation values

Response	Optimum parameters	Predicted value	Actual value	FEM value	Error %	
					FEM and predicted values	Actual and predicted values
Displacement	A5B5C1	0.276 mm	0.284 mm	0.291 mm	5.4 %	2.8 %
Frequency		1261.562 Hz	1293.812 Hz	1031.254 Hz	3.1 %	2.5 %
GRG		0.5185	0.5334	0.5467	5.4 %	2.8 %

modelling the relationship between design parameters, two responses and grey relational grade. Entropy measurement technique was applied for calculating the weight factor corresponding to each response. ANOVA was performed to determine the significant parameters affecting the grey relational analysis. ANOVA and confirmation tests were then conducted to validate the statistical adequacy and the prediction accuracy of the developed mathematical models, respectively. The results indicated that the developed mathematic models have a good statistical adequacy and prediction accuracy.

The optimal combination of design variables was determined based on the main effect analysis. The optimal performances of the 2-DOF flexure-based mechanism were also obtained. The confirmation results indicated that the grey relational grade falls within 95 % of the confidence interval. The efficiency of proposed hybrid approach has been successfully proven by the experiments and simulations. The proposed methodology is useful for the multi-objective optimal design for related flexure-based mechanisms.

Acknowledgments The authors acknowledge and thank the Ministry of Science and Technology of the Republic of China for their partial financial support of this study under Contract Number: MOST 104-2221-E-151-010.

References

1. Teo, T.J.; Chen, I.M.; Yang, G.: A large deflection and high payload flexure-based parallel manipulator for UV nanoimprint lithography: Part II. Stiffness modeling and performance evaluation. Precis. Eng. **38**(4), 872–884 (2014)
2. Lin, W.; Chen, W.J.: Fiber assembly of MEMS optical switches with U-groove channels. IEEE Trans. Autom. Sci. Eng. **5**(2), 207–215 (2008)
3. Dickerson, S.M.; Hogan, J.M.; Sugarbaker, A.; Johnson, D.M.; Kasevich, M.A.: Multiaxis inertial sensing with long-time point source atom interferometry. Phys. Rev. Lett. **111**(8), 083001 (2014)
4. Li, Y.M.; Xu, Q.S.: A novel piezoactuated xy stage with parallel, and stacked flexure structure for micro-/nanopositioning. IEEE Trans. Ind. Electron. **58**(8), 3601–3615 (2011)
5. Huang, J.M.; Li, Y.M.: Design and analysis of a completely decoupled compliant parallel XY micro-motion stage. In: Proceedings of the IEEE International Conference on Robotics and Biomimetics, Tianjin, China, pp. 1008–1013 (2010)
6. Li, Y.M.; Huang, J.M.; Tang, H.A.: Compliant parallel xy micromotion stage with kinematic decoupling. IEEE Trans. Autom. Sci. Eng. **9**(3), 338–553 (2012)
7. Wu, Z.G.; Li, Y.M.; Zhao, X.H.: Comparative analysis of a 2-dof micro-stage with two different types of hinges based on level amplified principle. In: Proceeding of the IEEE International Conference on Automation and Logistics, Zhengzhou, China, pp. 405–410 (2012)
8. Xu, Q.S.: Mechanism design and analysis of a novel 2-dof compliant modular microgripper. In: 7th IEEE Conference on Industrial Electronics and Applications (ICIEA), pp. 1966–1971 (2012)
9. Tang, H.; Li, Y.M.: Design, analysis, and test of a novel 2-dof nanopositioning system driven by dual mode. IEEE Trans. Robot. **29**(3), 650–662 (2013)
10. Bhagat, U.; Shirinzadeh, B.; Clark, L.; Qin, Y.D.; Tian, Y.L.; Zhang, D.W.: Experimental investigation of robust motion tracking control for a 2-dof flexure-based mechanism. IEEE/ASME Trans. Mechatron. **19**(6), 1737–1745 (2014)
11. Eskandari, A.; Ouyang, P.R.: Design and optimization of a xy compliant mechanical displacement amplifier. Mech. Sci. **4**, 303–310 (2013)
12. Xu, Q.S.: Design and development of a flexure-based dual-stage nanopositioning system with minimum interference behavior. IEEE Trans. Autom. Sci. Eng. **9**(3), 554–562 (2012)
13. Li, Y.M.; Xu, Q.S.: Design of a new decoupled xy flexure parallel kinematic manipulator with actuator isolation. In: IEEE/RSJ International Conference on Intelligent Robots and Systems, pp. 470–475 (2008)
14. Li, Y.M.; Xu, Q.S.: Design and analysis of a totally decoupled flexure-based xy parallel micromanipulator. IEEE Trans. Robot. **25**(3), 645–656 (2009)
15. Tang, H.; Li, Y.M.: Optimal design, modeling and analysis of a 2-dof nanopositioning stage with dual-mode: towards high-rate AFM scanning. In: Intelligent Robots and Systems. Vilamoura, Algarve, Portugal, pp. 658–663 (2012)
16. Dao, T.P.; Huang, S.C.: Robust design for a flexible bearing with 1-dof translation using the Taguchi method and the utility concept. J. Mech. Sci. Technol. **29**(8), 3309–3320 (2015)
17. Tsao, C.C.; Hocheng, H.: Evaluation of thrust force and surface roughness in drilling composite material using Taguchi analysis and neural network. J. Mater. Proces. Technol. **203**, 342–348 (2008)
18. Altan, M.: Reducing shrinkage in injection moldings via the Taguchi, ANOVA and neural network methods. Mater. Des. **31**, 599–604 (2010)
19. Tzeng, Y.F.; Chen, F.C.: Multi-objective optimisation of high-speed electrical discharge machining process using a Taguchi fuzzy-based approach. Mater. Des. **28**, 1159–1168 (2007)
20. Pandey, A.K.; Dubey, A.K.: Taguchi based fuzzy logic optimization of multiple quality characteristics in laser cutting of duralumin sheet. Opt. Lasers Eng. **50**, 328–335 (2012)
21. Ulas, C.; Ahmet, H.A.: Use of the grey relational analysis to determine optimum laser cutting parameters with multi-performance characteristics. Opt. Laser Technol. **40**, 987–994 (2008)
22. Tsai, M.J.; Li, C.H.: The use of grey relational analysis to determine laser cutting parameters for QFN packages with multiple performance characteristics. Opt. Laser Technol. **41**, 914–921 (2009)
23. Chiang, Y.M.; Hsieh, H.H.: The use of the Taguchi method with grey relational analysis to optimize the thin-film sputtering process with multiple quality characteristic in color filter manufacturing. Comput. Indus. Eng. **56**, 648–661 (2009)
24. Wen, K.L.; Chang, T.C.; You, M.L.: The grey entropy and its application in weighting analysis. Syst., Man, Cybern. IEEE Int. Conf. **2**, 1842–1844 (1998)
25. Kumar, S.; Kumar, P.; Shan, H.S.: Effect of evaporative pattern casting process parameters on the surface roughness of Al–7 % Si alloy castings. J. Mater. Proces. Technol. **182**, 615–623 (2007)
26. Aggarwal, A.; Singh, H.; Kumar, P.; Singh, M.: Optimizing power consumption for CNC turned parts using response surface methodology and Taguchi's technique-A comparative analysis. J. Mater. Proces. Technol. **200**, 373–384 (2008)
27. Dubey, A.K; Yadava, V.: Multi-objective optimisation of laser beam cutting process. Opt. Laser Technol. **40**, 562–570 (2008)
28. Dao, T.P.; Huang, S.C.: Design, fabrication, and predictive model of a 1-dof translational, flexible bearing for high precision mechanism. Trans. Can. Soc. Mech. Eng. **39**(3), 419–429 (2015)
29. Ilo, S.; Just, C.; Xhiku, F.: Optimisation of multiple quality characteristics of hardfacing using grey-based Taguchi method. Mater. Des. **33**, 459–468 (2012)
30. Senthilkumar, N.; Tamizharasan, T.; Anandakrishnan, V.: Experimental investigation and performance analysis of cemented carbide

inserts of different geometries using Taguchi based grey relational analysis. Measurement **58**, 520–536 (2014)
31. Muthuramalingam, T.; Mohan, B.: Application of Taguchi-grey multi responses optimization on process parameters in electro erosion. Measurement **58**, 495–502 (2014)
32. Kuo, C.F.J.; Su, T.L.; Jhang, P.R.; Huang, C.Y.; Chiu, C.H.: Using the Taguchi method and grey relational analysis to optimize the flat-plate collector process with multiple quality characteristics in solar energy collector manufacturing. Energy **36**, 3554–3562 (2011)
33. Datta, S.; Nandi, G.; Bandyopadhyay, A.: Application of entropy measurement technique in grey based Taguchi method for solution of correlated multiple response optimization problems: A case study in welding. J. Manuf. Syst. **28**, 55–63 (2009)
34. Sharma, A.; Yadava, V.: Modelling and optimization of cut quality during pulsed Nd: YAG laser cutting of thin Al-alloy sheet for straight profile. Opt. Laser Technol. **44**, 159–168 (2012)
35. Shigley, J.E.; Mischke, C.R.: Mechanical Engineering Design. McGraw-Hill International Editions, New York (2001)
36. Howell, L.L.: Compliant Mechanisms. Wiley, New York (2001)
37. Montgomery, D.C.: Design and Analysis of Experiments. Wiley, New York (1997)
38. Phillip, R.: Taguchi Techniques for Quality Engineering. MCgraw-Hill, New York (1996)